ISSN 1063-7397, Russian Microelectronics, 2021, Vol. 50, No. 5, pp. 333–338. © Pleiades Publishing, Ltd., 2021.
Russian Text © The Author(s), 2021, published in Mikroelektronika, 2021, Vol. 50, No. 5, pp. 370–375.

Thin-Film Solid State Lithium-Ion Batteries of the $LiCoC_2$/LiPON/Si@O@Al System

A. S. Rudy[a], *, A. A. Mironenko[a], V. V. Naumov[a], I. S. Fedorov[a], A. M. Skundin[b], and Yu. S. Tortseva[a], **

[a] *Demidov Yaroslavl State University, Yaroslavl, 150003 Russia*

[b] *Frumkin Institute of Physical Chemistry and Electrochemistry, Russian Academy of Sciences, Moscow, 119071 Russia*

**e-mail: rudy@uniyar.ac.ru*

***e-mail: tortseva.julia@mail.ru*

Received February 18, 2021; revised March 22, 2021; accepted March 22, 2021

Abstract—Experimental samples of solid-state thin-film lithium-ion batteries (STLIBs) of the $LiCoO_2$/LiPON/Si@O@Al electrochemical system are manufactured using traditional mask technology by radio frequency magnetron sputtering of both the electrodes and electrolyte. The obtained samples have a specific capacity corresponding to the modern published data on industrial STLIB samples. The developed STLIB samples are capable of long (about 1000 cycles) cycling with an acceptable loss of capacity, provided that the charging voltage is limited to 3.7 V. Exceeding the charging voltage leads to an increase in the charging capacity, but to a noticeable acceleration of degradation during cycling. At cycling currents over 20 $\mu A/cm^2$, the inverse proportionality between the current and the discharge capacity is observed, which is determined by the delayed solid-phase diffusion of lithium. With a decrease in the cycling current, the discharge capacity approaches the theoretical capacity.

DOI: 10.1134/S106373972105005X

INTRODUCTION

Recently, the demand for portable and wearable electronics such as smartphones, smart cards, RFID tags, wrist gadgets, transdermal patches, and implants, has grown significantly. The only possible power sources for these devices are still lithium-ion batteries with the required dimensions and specific capacity. However, conventional lithium-ion batteries with a liquid electrolyte are no longer sufficiently miniaturized for wearable electronics and too unreliable for implants. Therefore, in the past decade, there has been an increased demand for solid-state thin-film lithium-ion batteries (STLIBs) [1–6]. Manufacturers of battery products are aiming to develop thin (less than 1 mm thick) STLIBs. The battery size is reduced through the use of the thin-film (1–3 microns) electrodes and solid electrolyte, the thickness of which does not exceed 1 micron.

Reducing the size of batteries entails a decrease in their specific energy consumption. The main reasons for the decrease in energy consumption are the contact phenomena at the solid-phase boundaries of the functional layers and the higher resistivity of a solid electrolyte compared to a liquid one. Therefore, when developing a technology for manufacturing STLIBs, the main task is to improve the adhesion of the functional layers and reduce the thickness of the solid electrolyte. Below we describe the laboratory technology for manufacturing experimental STLIB samples of the $LiCoO_2$/LiPON/Si@O@Al electrochemical system and the results of measuring their charge-discharge characteristics. The technological parameters affecting the discharge capacity of the STLIB experimental samples are discussed.

Experimental STLIB samples of the $LiCoO_2$/LiPON/Li electrochemical system were described at the end of the last century [7, 8]. Replacing lithium metal with a silicon composite leads to a significant simplification of the STLIB fabrication technology. Silicon composites are characterized by a high specific capacity. Electrodes based on the Si@O@Al composite were developed and investigated earlier [9, 10].

1. PRODUCTION OF EXPERIMENTAL STLIB SAMPLES

All the experimental STLIB samples had the same structure (Fig. 1) and differed only in the order of the arrangement of the anode and cathode relative to the substrate.

Batches of experimental samples were prepared by radio frequency magnetron sputtering on an SCR 651 Tetra setup using mask technology. For this, masks were made of steel and copper with a thickness of 0.5 to 0.8 mm. The lateral size of the masks was 100×100 mm^2,

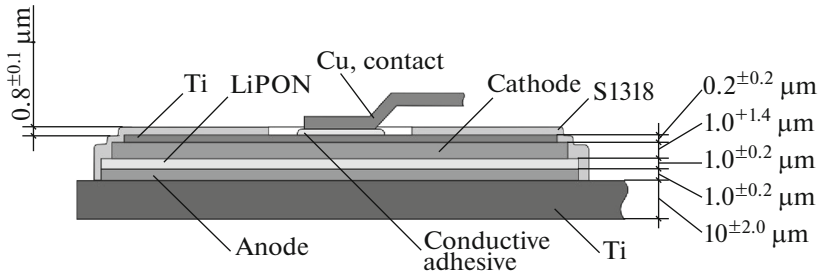

Fig. 1. The structure of the STLIB experimental samples.

while the masked windows had different sizes, which made it possible to create experimental STLIB samples of different areas. The constructive base of all the investigated STLIBs was made of titanium foil 10 μm thick. The substrate was preliminarily treated in an aqueous solution containing 5% sulfuric and 4% hydrofluoric acids with the formation of a surface relief to improve the adhesion of the substrate to the functional layer. Immediately before the application of the functional layer, the substrate was subjected to cleaning by ion bombardment. The Si@O@Al composite layer was deposited using two targets: from the Si–Al alloy (9 : 1) and pure aluminum; in this case, argon with an admixture of 0.3% oxygen served as the working gas.

Solid electrolyte (LiPON) was applied using Li_3PO_4. The target was made of Li_3PO_4 powder by the method of gradient pressing followed by annealing. To prevent cracking, the target was fixed in a copper holder, which ensured the uniform temperature distribution and efficient heat dissipation during sputtering. The working gas in this case was nitrogen. The technology of solid electrolyte deposition is described in detail in [11, 12].

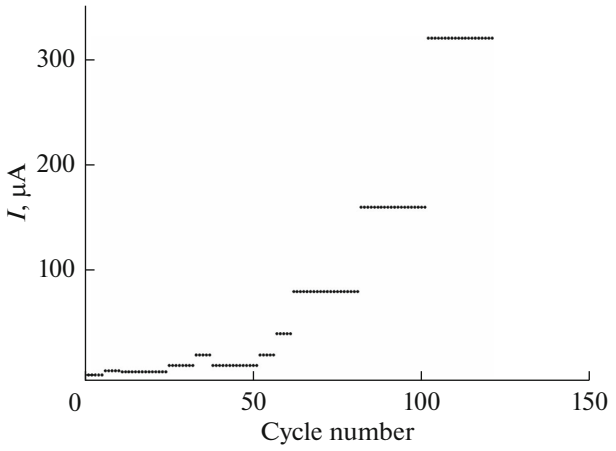

Fig. 2. Scheme of galvanostatic tests.

An $LiCoO_2$ layer was applied using a commercial target manufactured by OOO Girmet (Russia). An argon-oxygen mixture (4 : 1) served as the working gas.

2. TESTS OF EXPERIMENTAL STLIB SAMPLES

A freshly prepared STLIB sample is in the discharged state. This makes it possible to evaluate its characteristics both in the transient and practically stationary modes. The galvanostatic cycling of the STLIB samples with different currents and different voltages of the end of the charge and discharge was carried out using an automated AZRIVK 0.05A-5V charge-discharge measuring and computing complex manufactured by NTC Booster (Russia). Since the thickness of the active material of the positive and negative electrodes is the same (1 μm), and the specific capacity of the Si@O@Al composite is more than an order of magnitude higher than the specific capacity of $LiCoO_2$, the samples under study were cathode-limited.

Figure 2 shows the typical cyclic test setup. The current cycling is shown here. It can be seen that at the very beginning of the tests, the charge and discharge were carried out with a sufficiently low current, so that the total state of the charge of the sample in the first 25 cycles was insignificant and, at the same time, increased from cycle-to-cycle. This stage of research corresponded to the transitional regime. In the last cycles (60–120), the state of charge of the STLIB was close to the limiting one, and this stage can be considered as stationary. The surface area of the electrodes in this STLIB sample was 2.64 cm^2.

2.1. STLIB Characteristics in the Transient Mode

It has already been indicated that the positive electrode was the limiter of the capacitance in the investigated STLIB samples. The current-generating reaction on the $LiCoO_2$ electrode is known to have the form

$$LiCoO_2 \leftrightarrow Li_{1-x}CoO_2 + xLi^+ + xe. \quad (1)$$

Extracting all lithium when charged ($x = 1$) corresponds to the theoretical specific capacity of 273 mAh/g. However, with such a full charge, irreversible struc-

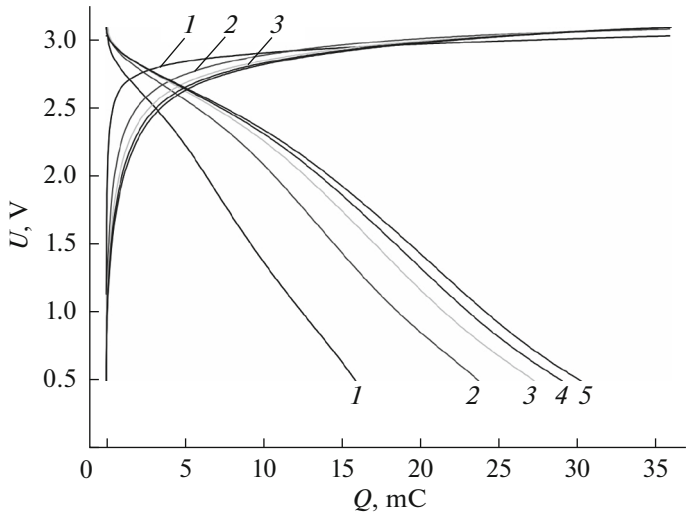

Fig. 3. Charging and discharging curves for the first five cycles. The cycle numbers are shown in the figure.

tural changes occur, and in reality the charge is carried out up to values $x \approx 0.5$, and the real reversible capacity does not exceed 150 mAh/g [13]. In the considered STLIB, the amount of $LiCoO_2$ on the electrode is 0.6 mg (electrode area 2.64 cm^2, layer thickness 1 μm, density $LiCoO_2$ 2.3 g/cm^3). Thus, the theoretical capacity of the electrode (and the entire STLIB) is 164 μAh (590 μC), and the capacity for reliable reversible cycling should not exceed ≈300 μC. A charge significantly exceeding this value can lead to the accelerated degradation of the electrode.

Figure 3 shows the charging and discharging curves corresponding to the first five cycles at a cycling current of 1 μA. In this case, the charge was limited to 36 mC, and the final charge voltage did not exceed 3.09 V.

As can be seen, when such a small charge is applied in the first cycle, the distribution of the lithium concentration over the thickness of the electrodes turns out to be quite uniform, the deviation of the lithium concentration from the limiting values is insignificant, and during the first discharge, even up to such a small final voltage (0.5 V), less than half of the capacitance is extracted in the charge. In the second cycle, with the same amount of electricity supplied during charging, a large capacity is extracted during the discharge, and as the cycle progresses, the excess of the charging capacity over the discharge capacity decreases (Fig. 4).

In cycles 6–10 at a charge and discharge current of 5 μA, the same regularity was qualitatively observed: as the cycling progressed, the excess of the charging capacity over the discharge capacity noticeably decreased.

In cycles 11–24, the charge and discharge current was somewhat reduced, and the cycling took place practically in a stationary mode. Here the discharge capacity did not differ from the charging one. With a further increase in the charge and discharge current to 10 μA (25–32 cycles), the mode again became transient. Typically, at 25–32 cycles, the charging capacity increased to 360 mC, which exceeded the recommended limit by 20%. As can be seen from Fig. 4, such an excess of the charging capacity had not yet led to irreversible structural changes in $LiCoO_2$ or to a noticeable degradation of the STLIB.

Starting from the 33rd cycle, the test program was changed: in this case, the charge was carried out not to a constant capacity, but to a predetermined final voltage of 4.0 V. In this mode, at the 33rd cycle, the charging capacity was 465 mC, which led to a subsequent noticeable degradation. Figure 5 shows the charging and discharging curves of cycles 33–37 when the charging and discharging current was 20 μA. At this stage, as the cycle progressed, both the charging and discharging capacities decreased, but their difference (starting from the 34th cycle) barely changed (Fig. 6).

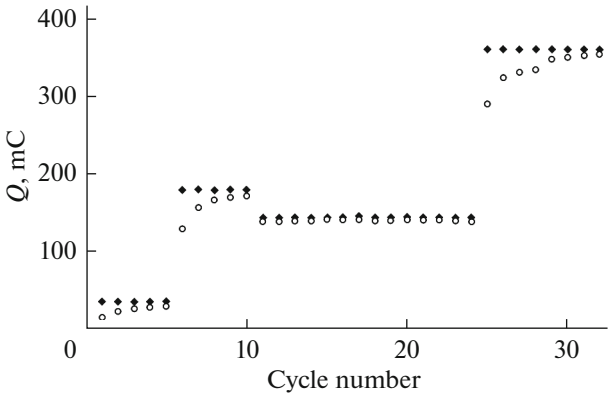

Fig. 4. Changing the charging (black diamonds) and discharge (circles) capacities during cycling in the transient mode.

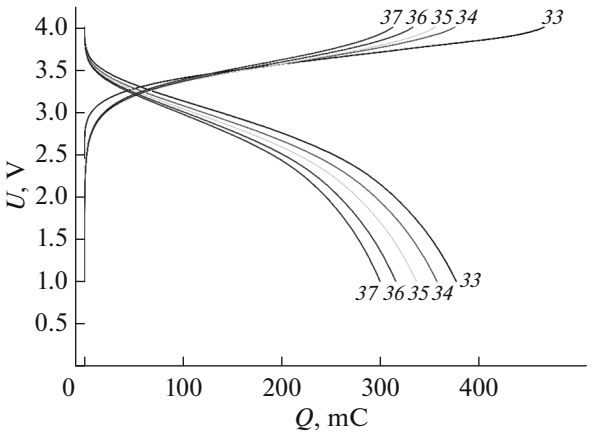

Fig. 5. Charging and discharge curves 33–37 cycles. The cycle numbers are shown in the figure.

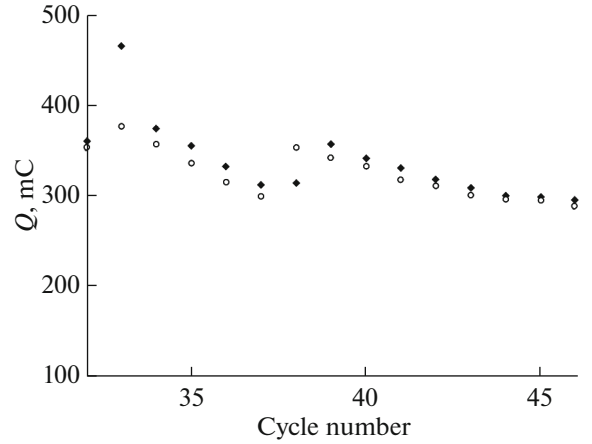

Fig. 6. Changing the charging (black rhombuses) and discharge (white circles) capacities when cycling with a current of 20 μA (33–37 cycles) and 10 μA (38–46 cycles).

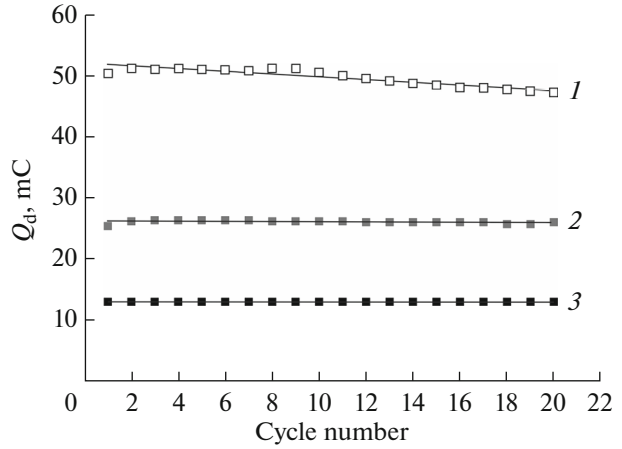

Fig. 7. The change in capacitance during cycling in a stationary mode at currents of 80 μA (*1*), 160 μA (*2*), and 320 μA (*3*).

Starting from cycle 38, the current was reduced to 10 μA, while maintaining the final charge voltage of 4.0 V. As can be seen from Fig. 6, the rate of degradation decreased, and the system came to an almost stationary state.

2.2. STLIB Characteristics in the Stationary Mode

When cycling in the stationary mode, the charging capacity practically did not differ from the charging capacity. Three series of 20 cycles were carried out with currents of 80, 160, and 320 μA at a final charge voltage of 3.7 V. The decrease in the final charge voltage led, of course, to a certain decrease in the charging capacity, but guaranteed against structural changes during cycling. Figure 7 shows the change in the discharge capacity during cycling in these series.

The straight lines in Fig. 7 were drawn using the least squares method. The slope of these straight lines corresponds to the degradation rate, which was 0.223 mC/cycle (or 0.43% per cycle) for cycling with a current of 80 μA, 0.0148 mC/cycle (or 0.056% per cycle) at a current of 160 μA, and was lower than the measurement sensitivity at a current of 320 μA. Such a weak degradation during cycling made it possible to evaluate the effect of the cycling current on the capacitance (subject to charging and discharging to fixed values of the final voltage). This assessment also took into account shorter tests at currents of 10, 20, and 40 μA.

Figure 8 shows the charging and discharging curves obtained at different currents. The increase in the current leads to an obvious decrease in capacitance, which is determined by the slowness of the diffusion of lithium in the solid phase of the active materials of the electrodes ($LiCoO_2$ and Si@O@Al). It is characteristic that the shape of the curves does not change when the current changes, which is especially clearly seen when these curves are presented in normalized coordinates (Fig. 9), when the fraction of the capacitance from the maximum achieved in this process is plotted along the abscissa axis rather than the absolute capacitance [14].

The results shown in Fig. 8 make it possible to reveal the quantitative dependence of the capacitance on the cycling current. This dependence is shown in the discharge capacity–reverse current coordinates in Fig. 10. It can be seen that at currents exceeding 40 μA, the discharge capacity is inversely proportional to the current, which confirms the assumption about the diffusion nature of the limiting stage of the process. Indeed, under galvanostatic conditions at relatively low current densities, lithium penetrates the entire depth of the active layer of the electrode. With an increase in the current density, by the time the final voltage is reached (i.e., when the time of the galvanostatic experiment is equal to the transient time τ), the thickness of the diffusion layer becomes less than the thickness of the active layer and the discharge capacity turns out to be less than the limiting one. The transi-

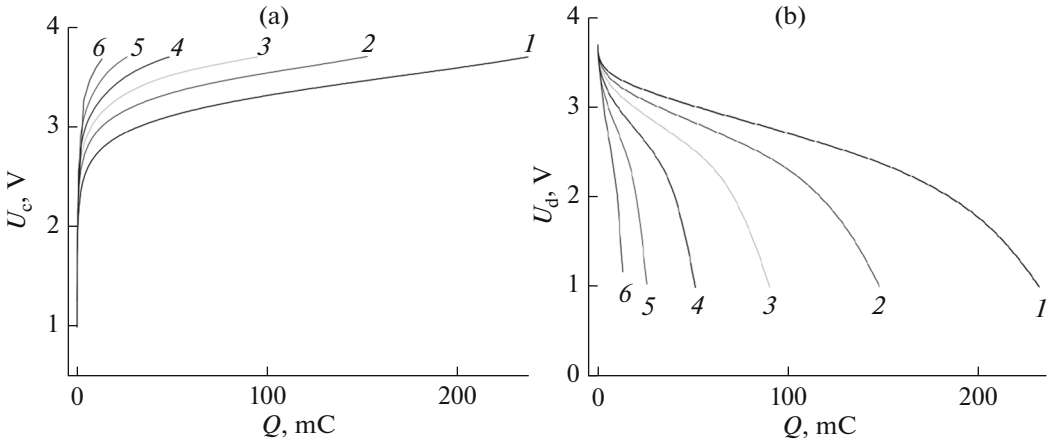

Fig. 8. Charging (a) and discharge (b) curves obtained at currents of 10 μA (*1*), 20 μA (*2*), 40 μA (*3*), 80 μA (*4*), 160 μA (*5*), and 320 μA (*6*).

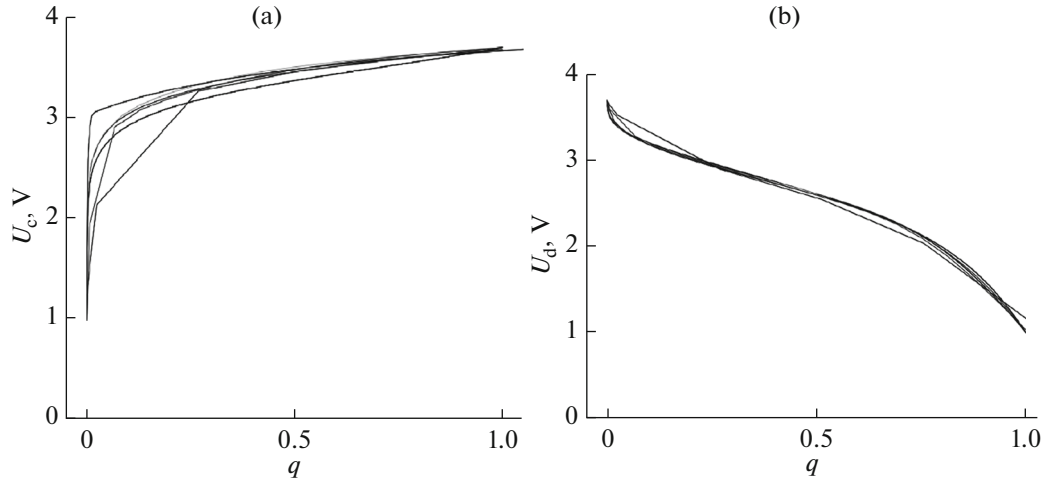

Fig. 9. Curves in Fig. 8 in normalized coordinates.

tion time under conditions of flat semi-infinite diffusion is determined by the expression [15]

$$\tau = \pi n^2 F^2 D c^2 / 4 i^2, \quad (2)$$

where i is the current density, n is the number of electrons participating in the discharge reaction carried by the diffusing particle, c and D are the concentration and diffusion coefficient of the diffusing particles, and F is the Faraday constant.

Under galvanostatic conditions, the capacitance is equal to the product of current and time; therefore, Eq. (2) can be represented as

$$Q = \pi n^2 F^2 D c^2 / 4 i, \quad (3)$$

which confirms the inverse proportional relationship between the capacity and current.

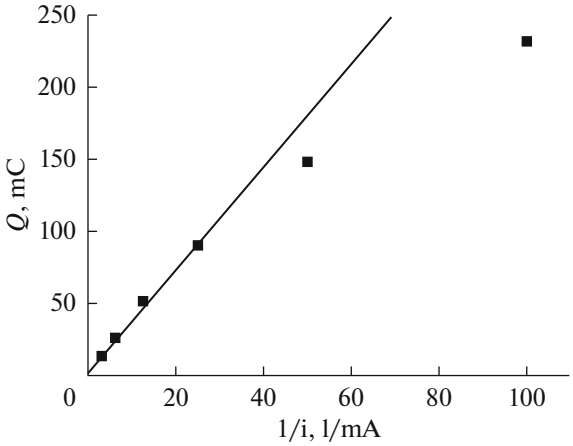

Fig. 10. Dependence of the discharge capacity on the current.

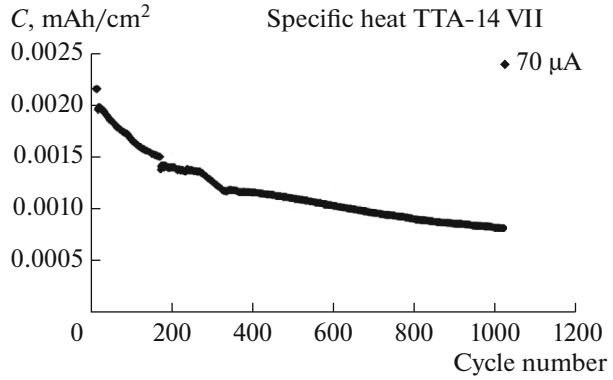

Fig. 11. Change in the discharge capacity of a STLIB sample with an electrode area of 1.44 cm^2 in long cycling.

At cycling currents less than 40 μA, obviously, the thickness of the diffusion layer exceeds the thickness of the active material on the electrodes, and semi-infinite diffusion transforms into limited diffusion, which causes a deviation from the straight line in Fig. 10.

To assess the possibilities of stable cycling, long-term galvanostatic tests were carried out with an STLIB sample with an electrode area of 1.44 cm^2. The tests were carried out at a charge and discharge current of 70 μA (this mode corresponded to a current of 130 μA for the STLIB sample described above) and the final charge and discharge voltages of 3.7 and 1.0 V. The results of long-term tests are shown in Fig. 11.

It can be seen that the degradation rate at the first stage (initial 320 cycles) was 0.13% per cycle and then decreased to a level of 0.04% per cycle. These results are, in general, consistent with those given above for a different STLIB sample.

FUNDING

This study was supported by the Ministry of Science and Higher Education of the Russian Federation as part of state assignment no. 0856-2020-0006 of Demidov Yaroslavl State University using the equipment of the Center for Collective Use "Diagnostics of micro- and nanostructures."

CONFLICT OF INTEREST

The authors declare that they have no conflict of interest.

REFERENCES

1. Sun, C., Liu, J., Gong, Y., Wilkinson, D.P., and Zhang, J., Recent advances in all-solid-state rechargeable lithium batteries, *Nano Energy,* 2017, vol. 33, p. 363.
2. Patil, A., Patil, V., Shin, D.W., Choi, J.-W., Paik, D.-S., and Yoon S.-J., Issue and challenges facing rechargeable thin film lithium batteries, *Mater. Res. Bull.,* 2008, vol. 43, p. 1913.
3. Souquet, J.L. and Duclot, M., Thin film lithium batteries, *Solid State Ionics,* 2002, vol. 148, p. 375.
4. Bates, J.B., Dudney, N.J., Neudecker, B., Ueda, A., and Evans, C.D., Thin-film lithium and lithium-ion batteries, *Solid State Ionics,* 2000, vol. 135, p. 33.
5. Jones, S.D. and Akridge, J.R., Thin film rechargeable Li batteries, *Solid State Ionics,* 1994, vol. 69, p. 357.
6. Dudney, N.J., Thin film micro-batteries, *Electrochem. Soc. Interfaces,* 2008, vol. 3, p. 44.
7. Bates, J.B., Dudney, N.J., Lubben, D.C., Gruzalski, G.R., Kwak, B.S., Xiaohua, Yu., and Zuhr, R.A., Thin-film recharge-able lithium batteries, *J. Power Sources*, 1995, vol. 54, p. 58.
8. Wang, B., Bates, J.B., Hart, F.X., Sales, B.C., Zuhr, R.A., and Robertson, J.D., Characterization of thin-film rechargeable lithium batteries with lithium cobalt oxide cathodes, *J. Electrochem. Soc.,* 1996, vol. 143, p. 3203.
9. Kulova, T.L., Skundin, A.M., and Andreev, V.N., Gryzlov, D.Yu., Mironenko, A.A., Rudyi, A.S., Gusev, V.N., and Naumov, V.V., Cyclic voltammetry studies of silicon-aluminum thin-film electrodes synthesized in the presence of oxygen, *Russ. J. Electrochem.,* 2015, vol. 51, p. 1157.
10. Kulova, T.L., Mironenko, A.A., Skundin, A.M., Rudy, A.S., Naumov, V.V., and Pukhov, D.E., Study of silicon composite for negative electrode of lithium-ion battery, *Int. J. Electrochem. Sci.,* 2016, vol. 11, p. 1370.
11. Vasilev, S.V., Lebedev, M.E., Mazaletskii, L.A., Metlitskaya, A.V., Mironenko, A.A., Naumov, V.V., Novozhilova, A.V., Rudyi, A.S., and Fedorov, I.S., Development of the technology of magnetron sputtering deposition of LiPON films and investigation of their characteristics, *Russ. Microelectron.,* 2017, vol. 46, p. 424.
12. Rudyi, A.S., Vasil'ev, S.V., Metlitskaya, A.V., Novozhilova, A.V., Churilov, A.B., Lebedev, M.E., Mironenko, A.A., Naumov, V.V., and Fedorov, I.S., An experimental examination of thin films of lithium phosphorus oxynitride (a solid electrolyte), *Tech. Phys. Lett.,* 2017, vol. 43, p. 503.
13. *Lithium Batteries: Science and Technology,* Nazri, G.-A. and Pistoia, G., Eds., New York: Springer, 2009.
14. Kulova, T.L. and Skundin, A.M., A simple method to diagnose the causes of electrode degradation when cycling lithium-ion batteries, *Elektrokhim. Energet.,* 2011, vol. 11, p. 171.
15. Galus, Z., *Teoretyczne Podstawy Elektroanalizy Chemicznej,* Warszawa: Panstwowewidawnictwonaukowe, 1971.